WAVELET FRAME BASED SEISMIC ATTRIBUTES EXTRACTION USING A FILTERING SCHEME

PING WANG[1,2] and JINGHUAI GAO[1,2]

[1] *Institute of Wave and Information, Xi'an Jiaotong University, 710049 Xi'an, P.R. China.*
skyey.xjtu@gmail.com
[2] *National Engineering Laboratory for Offshore Oil Exploration, 710049 Xi'an, P.R. China.*

ABSTRACT

Wang, P. and Gao, J., 2013. Wavelet frame based seismic attributes extraction using a filtering scheme. *Journal of Seismic Exploration*, 22: 353-372.

   Extraction of instantaneous attributes is important for seismic data processing and interpretation. However, the instantaneous attributes extracted by the conventional Hilbert transform method are sensitive to noise that inevitably lies in field seismic data. We propose a robust approach to extract instantaneous attributes in wavelet domain. In the proposed approach, we apply a superfamily of analytic wavelets with some desirable properties-the generalized Morse wavelets-in the proposed approach. Based on the proposed discretization, the wavelet family can constitute a tight frame. For signal in noise, we implement a filtering scheme to determine the distribution of the effective signal in the transformed domain before calculating the instantaneous attributes. In this filtering scheme, a percentage thresholding strategy is manipulated. Compared with the conventional method based on Hilbert transform, the synthetic trace and real data examples show higher precision and anti-noise performance of the proposed approach, even for signals contaminated by strong noise.

KEY WORDS: instantaneous attributes, anti-noise, Hilbert transform, tight frame,
                generalized Morse wavelet, filtering scheme, soft-thresholding.

INTRODUCTION

   Geological interpretation of seismic data is commonly done by analyzing patterns of seismic attributes across a prospect area. Although many seismic attributes have been utilized to emphasize geologic targets and to define critical rock and fluid properties, these three simple attributes-instantaneous amplitude, instantaneous phase and instantaneous frequency-remain the mainstay of geological interpretation of seismic data (Hardage, 2010).

Instantaneous amplitude is often associated with lithological changes between adjacent rock layers and hydrocarbon accumulation. Instantaneous phase are effective in showing discontinuities, faults, pinch outs, angularities and seismic sequence boundaries. Instantaneous frequency provides a useful correlation tool to delineate the thickness or lithology changes of the layers. The changes of instantaneous frequency can be used to indicate the distribution of hydrocarbon (Taner et al., 1979). The instantaneous attributes have successful applications in subsurface structure analysis (Chopra and Marfurt, 2005) and seismic parameter inversion such as quality (Q) factor (Yang and Gao, 2010; Gao et al., 2011).

After the work of Gabor (1946) and Ville (1948), a great number of papers have been published on instantaneous attributes (Vakman, 1996; Picinbono, 1997) and a review was given by Boashash (1992). Taner et al. (1979) introduced complex trace analysis, in which the Hilbert transform (HT) is used to calculate seismic amplitude, phase and frequency instantaneously - meaning a value for each parameter is calculated at each time sample of a seismic trace. The HT method has been applied widely in seismic exploration (Barnes, 1992; Barnes, 1996; Taner, 2001; Fomel, 2007; Zhou et al., 2012). Estimating instantaneous attributes of seismic trace based on time-frequency representations has also been studied by several authors (Steeghs and Guy, 2001; Hardy et al., 2003; Huang and Milkereit, 2009; Han and van der Baan, 2011; Fomel, 2012; Wang and Gao, 2013).

The conventional Hilbert transform (HT) method now forms the basis by which almost all instantaneous attributes are calculated by today's seismic interpretation software. In the HT method, a seismic trace x(t) is converted into a complex seismic trace z(t), which consists of the real seismic trace x(t) and an imaginary seismic trace h(t) that is the Hilbert transform of x(t). However, this method is sensitive to noise, thus it brings difficulty for seismic attributes analysis, especially in a noisy environment.

In this paper, we present a wavelet-based approach using continuous wavelet transform (CWT) for the calculation of the analytic counterpart of a real-valued signal and its instantaneous attributes. A new class of analytic wavelets - the Generalized Morse wavelet (GMW) (Olhede and Walden, 2002; Lilly and Olhede, 2012), which substantially outperform the popular Morlet wavelet - is applied as the basic wavelet.

For numerical purposes, the scaling factor and the shifting factor of the CWT should be discretized in the scale-shift plane, thus a wavelet family can be obtained. Frames were first proposed by Duffin and Schaeffer (1952) which are now used in a wide range of applications. The frame is said to be tight if the upper and lower bounds are equal. The GMW family based on the proposed discretization scheme can constitute a tight frame. Furthermore, the GMW

family can constitute a tighter frame than the Morlet wavelet family based on the same discretization scheme (Wang and Gao, 2013). This provides a simple process of recovering the signal from its frame coefficients and the filtering scheme can be utilized in the following procedure.

When a signal in noise is transformed into time-scale domain using CWT, the energy distribution of the effective signal will be confined in a small close subspace of the time-scale domain, while the energy distribution of the noise may disperse in a larger close subspace, even in the whole time-scale space (Wang and Gao, 2013). To determine the distribution of the effective signal, we employ a filtering scheme. We first determine the range of the scaling factor and the shifting factor. Then, we apply a percentage thresholding strategy to obtain the coefficients corresponding to the effective signal in time-scale domain. Thus, the analytic counterpart of the effective signal can be calculated and the instantaneous attributes can also be estimated.

The paper starts with reviewing the conventional instantaneous attributes estimation method based on the Hilbert transform. Then, we propose the robust estimation approach. We introduce the method of calculating the analytic counterpart and instantaneous attributes of a real-valued signal by wavelet transform. We focus on the choice of wavelet and the discretization scheme. Owing to the desirable properties, the GMW is used in the proposed approach. In the following, we determine the distribution of the effective signal by the proposed filtering scheme and calculate the instantaneous attributes. Finally, the comparisons between the proposed approach and HT method, the performances of different thresholding strategy in the filtering scheme, also with the comparisons between the proposed approach using GMW and the Morlet wavelet, are presented by calculating instantaneous frequencies (IFs) of the signals. Experimental results on synthetic signals and real seismic data demonstrate the excellent performance of the proposed approach.

THE CONVENTIONAL HILBERT TRANSFORM METHOD

For a real-valued signal $x(t)$, the corresponding analytic signal, denoted as $z(t)$ can be defined as follows:

$$z(t) = x(t) + ih(t) \; , \tag{1}$$

where the imaginary part $h(t)$ is the Hilbert transform of $x(t)$. Then, the instantaneous attributes can be defined as

$$e(t) = \sqrt{\{x^2(t) + h^2(t)\}} \; , \quad \theta(t) = \arctan[h(t)/x(t)] \; ,$$

$$f(t) = (1/2\pi)(d/dt)\{\arctan[h(t)/x(t)]\} \; , \tag{2}$$

where e(t), θ(t) and f(t) represent the instantaneous amplitude (IA), instantaneous phase (IP), and instantaneous frequency (IF) of x(t), respectively. Note that the definition of instantaneous frequency calls for division of two signals:

$$f(t) = (1/2\pi)(d/dt)\{arctan[h(t)/x(t)]\}$$

$$= (1/2\pi)\{[x(t)h'(t) - x'(t)h(t)]/[x^2(t) + h^2(t)\} \quad . \tag{3}$$

In a linear algebra notion (Fomel, 2007)

$$f = D^{-1}v \quad , \tag{4}$$

where f represents the vector of instantaneous frequencies f(t), v represents the numerator in eq. (3), and D is a diagonal operator made from the denominator of eq. (3). A recipe for avoiding division by zero is adding a small constant ε to the denominator (Matheney and Nowack, 1995). Consequently, eq. (4) becomes

$$f_{inst} = (D + \varepsilon I)^{-1}v \quad , \tag{5}$$

where I stands for the identity operator. Stabilization by ε does not, however, prevent instantaneous frequency from being susceptible by noise.

PROPOSED ESTIMATION APPROACH

We get the analytic counterpart of a real-valued signal using wavelet transform instead of Hilbert transform. We use the generalized Morse wavelet (GMW) as a superior alternative to the popular Morlet wavelet. With the proposed discretization, the GMW family can constitute a tighter frame. For signals in noise, the distribution of effective signals in time-scale domain can be determined by the proposed filtering scheme.

Instantaneous attributes extraction by CWT

The continuous wavelet transform (CWT) of a signal x(t) $\in$ L$^2(\mathbb{R})$ is defined as

$$W_\psi(t,a) \equiv (1/a) \int_{-\infty}^{+\infty} x(\tau)\psi^*[(\tau - t)/a]d\tau \quad , \tag{6}$$

where ψ^*(t) corresponds to the complex conjugate of ψ(t). Note the normalization factor is chosen to be 1/a instead of the more common 1/$\sqrt{a}$, as

the former is more convenient for oscillatory signals (Lilly and Olhede, 2010). The wavelet function $\psi(t)$ is zero-mean and satisfies the admissibility condition (Holschneider and Kon, 1996): $K_\psi \equiv \int_{-\infty}^{+\infty} |\Psi(\omega)|^2/|\omega|\, d\omega < \infty$, where $\Psi(\omega) = \int_{-\infty}^{+\infty} \psi(t)e^{-i\omega t} dt$ is the Fourier transform of the wavelet.

The wavelet function is said to be analytic if $\Psi(\omega) = 0$ for $\omega < 0$. The following theorem was proved by Gao et al. (1999):

Theorem 1. If $\psi(t)$ is an analytic wavelet function with its real part being even and satisfies the admissibility condition, for an arbitrary signal $x(t) \in L^2(\mathbb{R})$, we have

$$c(t) \equiv (1/K_\psi) \int_0^\infty W_\psi(t,a)(da/a) = x(t) + ih(t) , \tag{7}$$

where $h(t)$ is the Hilbert transform of $x(t)$. Thus $c(t)$ is the analytic counterpart of the real-valued signal $x(t)$. Then, we compute instantaneous attributes:

$$\hat{e}(t) = \sqrt{\{Re^2[c(t)] + Im^2[c(t)]\}} ,$$

$$\hat{\theta}(t) = \arctan[Im[c(t)]/Re[c(t)]] , \tag{8}$$

$$\hat{f}(t) = (1/2\pi)(d/dt)\{\arctan[Im[c(t)]/Re[c(t)]]\} ,$$

where $Re[c(t)]$ and $Im[c(t)]$ are the real part and imaginary part of $c(t)$, while $\hat{e}(t)$, $\hat{\theta}(t)$ and $\hat{f}(t)$ represent the instantaneous amplitude (IA), instantaneous phase (IP), and instantaneous frequency (IF) calculated by the proposed approach, respectively. To avoid division by zero, the linear algebra form of IF, which is similar to eq. (5), can be given by

$$\hat{f}_{inst} = (D' + \varepsilon I)^{-1}v' . \tag{9}$$

Note the instantaneous attributes calculated direct using eqs. (6)-(9) are identical with that obtained by the conventional HT method. However, for noisy signal, when it is transformed into time-scale domain via eq. (6), we should determine the distribution of the effective signal before calculating the analytic counterpart using eq. (7).

Choice of wavelet

A commonly used complex-valued wavelet is the Morlet wavelet (Holschneider and Kon, 1996), which was first introduced by Morlet, and given by

$$\psi_\sigma(t) = a_\sigma e^{-(1/2)t^2}[e^{i\sigma t} - e^{-(1/2)\sigma^2}] \ , \tag{10}$$

$$\Psi_\sigma(\omega) = a_\sigma e^{-(1/2)(\omega-\sigma)^2}[1 - e^{-\omega\sigma}] \ , \tag{11}$$

where σ is the carrier wave frequency. The second term in eqs. (10) and (11) is a correction necessary to enforce zero mean, while a_σ normalizes the wavelet amplitude. For sufficiently large σ, e.g., $\sigma > 5.33$, the values of the second term are so small that they can be neglected. Meanwhile, the values of $\Psi_\sigma(\omega)$ for $\omega \leq 0$ are so small that ψ_σ can be considered as an analytic wavelet.

The generalized Morse wavelets (GMWs) are a two-parameter family of wavelets, defined, in the frequency domain, by Olhede and Walden (2002)

$$\Psi_{\beta,\gamma}(\omega) = U(\omega)\alpha_{\beta,\gamma}\omega^\beta e^{-\omega^\gamma} \ , \tag{12}$$
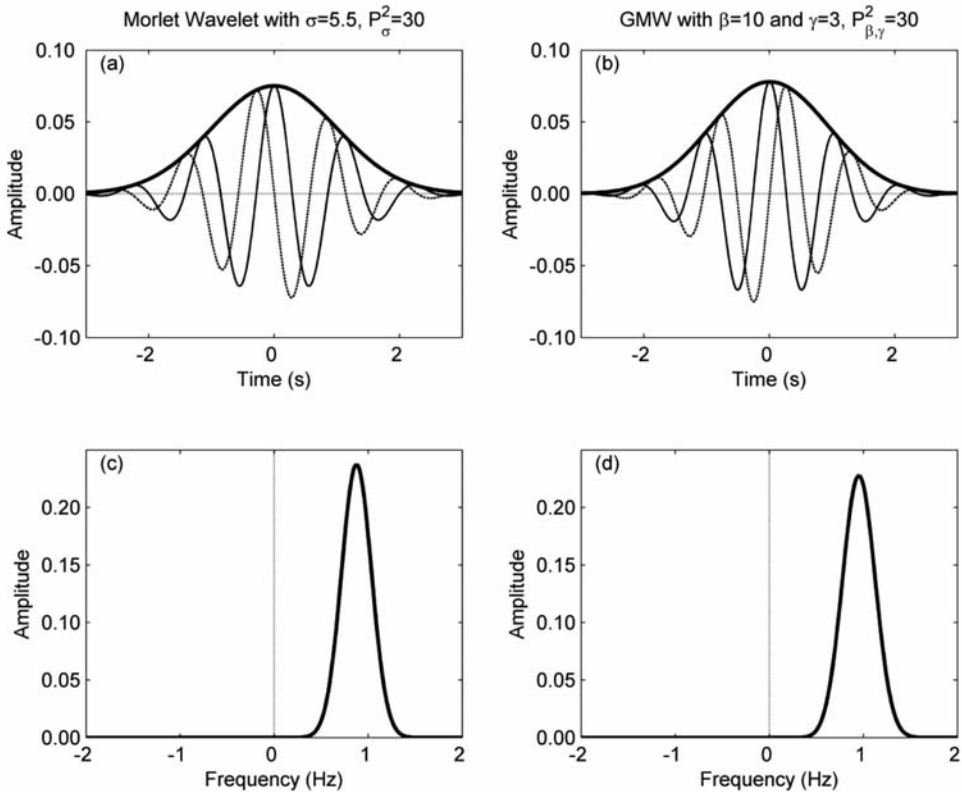

Fig. 1. (a) Morlet wavelet. (b) Generalized Morse wavelet. (c), (d) The wavelets in frequency-domain. In (a) and (b), the thick solid, thin solid, and dashed lines correspond to the magnitude, real part, and imaginary part of the time-domain wavelet, respectively.

where U(ω) is the Heaviside step function and $\alpha_{\beta,\gamma} \equiv 2(e\gamma/\beta)^{\beta/\gamma}$ is a normalizing constant. To be a valid wavelet, one must have $\beta > 0$ and $\gamma > 0$. The role of β and γ in controlling wavelet properties were investigated by Lilly and Olhede (2012).

Despite its usefulness, the Morlet wavelet suffers from some limits. On top of that, the Morlet wavelet is not, however, exactly analytic - it is only approximately analytic for sufficiently large σ. As an example, a generalized Morse wavelet and a Morlet wavelet, both in time-domain and frequency-domain, are shown in Fig. 1. Parameter settings have been chosen such that the time-domain length defined by Lilly and Olhede (2009) is the same for both wavelets. These two wavelets appear indistinguishable, and both of them are supported on the positive real-axis only in frequency-domain, i.e., are analytic. However, if we narrow the time window of both wavelets in order to increase time resolution, we obtain the wavelets shown in Fig. 2. The Morlet wavelet exhibits leakage to negative frequencies while the generalized Morse wavelets
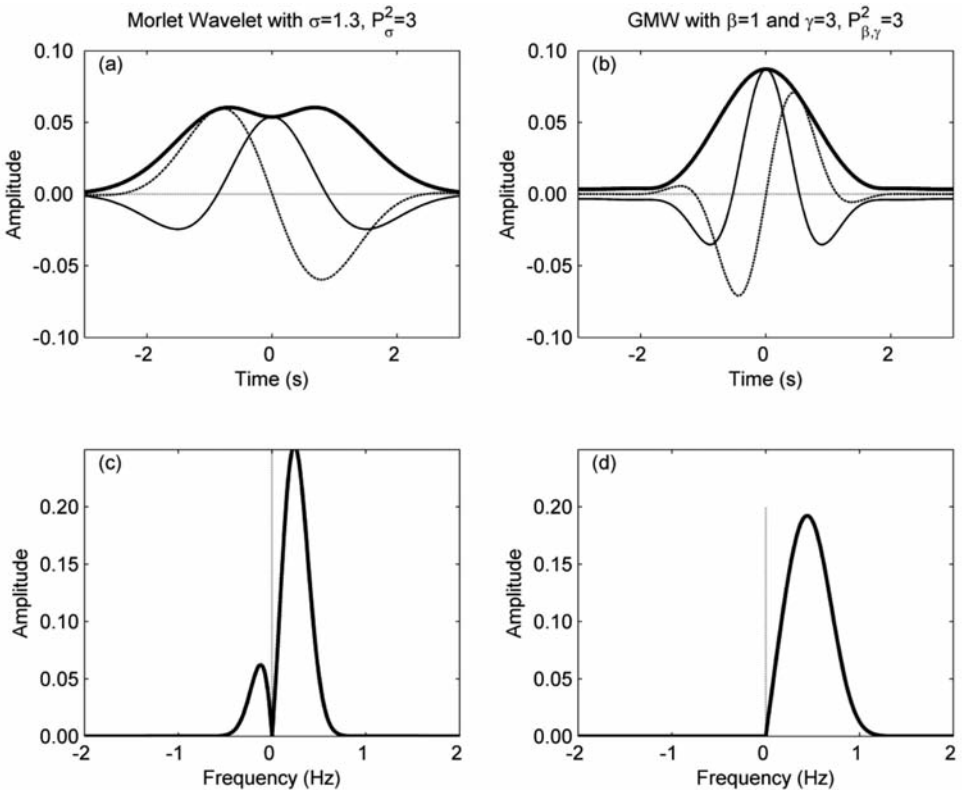

Fig. 2. As with Fig. 1, but for different parameter settings.

remain analytic even for highly time-localized parameter settings. The advantage of using precisely, as opposed to approximately analytic wavelets was demonstrated by Olhede and Walden (2003) and Lilly and Olhede (2009), who showed that even small amounts of leakage to negative frequencies can result in spurious variation of the transform phase. Besides, it is also important to point out that c(t) in eq. (7) is the analytic counterpart of the real-valued signal only if the wavelet is analytic, as stated in Theorem 1. The precision of instantaneous attribute obtained by using the Morlet wavelet is degraded because of its departure from analyticity.

Furthermore, the Morlet wavelet depends on just one parameter, implying that it is not versatile. By varying two parameters, the GMWs can be given a broad range of characteristics while remaining exactly analytic. Based on the proposed discretization scheme, the GMW family can constitute a tighter frame, which will be discussed in next section. Besides, the more similar is the basic wavelet and data to each other, the more concentrated the energy distribution in the time-scale domain. Comparing with Morlet wavelets, the GMWs allow for more flexibility by varying two parameters and can be selected to best match the data to be analyzed. The GMWs are used to calculate the analytic counterpart of a real-valued signal and its instantaneous attributes in the proposed approach.

The discretization scheme

In eq. (6), a wavelet atom is a translation by t and a dilation by a of a mother wavelet ψ:

$$\psi_{t,a}(\tau) = (1/a)\psi[(\tau - t)/a] \quad . \tag{13}$$

For numerical purposes, the scale factor a and the translation factor t must be discretized. In our discretization scheme, a is sampled along an exponential sequence $\{a_0^m\}$ with scale step $a_0 > 1$, t is sampled uniformly with intervals t_0, then the wavelet family can be obtained:

$$\psi_{m,n}(x) = a_0^{-m}\psi[a_0^{-m}(x - nt_0)] \quad . \tag{14}$$

In our implementation, t_0 is set equal to the sampling interval of the observed signal, thus the wavelet family is translation-invariant, obtained by translating a family of generators (Mallat, 2009): $\{\phi_m(x) = a_0^{-m}\psi(a_0^{-m}x)\}$. For translation-invariant dictionary, the following theorem was given (Mallat, 2009), which proves that the frame condition is equivalent to a condition on the Fourier transform $\Phi_m(\omega)$ of the generators $\phi_m(x)$.

Theorem 2

If there exit two constants $B \geq A > 0$ such that for almost all ω in ??

$$A \leq \sum_m |\Phi_m(\omega)|^2 \leq B , \qquad (15)$$

then the translation-invariant dictionary constitutes a frame. A and B are the lower and upper bounds for the frame. Since $\Phi_m(\omega) = \Phi(a_0^m \omega)$, the Fourier condition means

$$A \leq \sum_{m=-\infty}^{+\infty} |\Phi_m(a_0^m \omega)|^2 \leq B . \qquad (16)$$

To characterize the degree of tightness of a frame, a variable snugness (Antoine et al., 2004) is adopted:

$$\delta = (B - A)/(B + A) . \qquad (17)$$

A small δ means the upper bound B is close to the lower bound A, and the wavelet family approximately constitute a tight frame (Wang et al., 2012). The frame is tight when $\delta = 0$. We denote the power in frequency domain $\sum_{m=-\infty}^{+\infty} |\Psi_m(a_0^m \omega)|^2$ as $F_{a_0}(\omega)$, then we calculate $F_{a_0}(\omega)$ of the GMW family and the Morlet wavelet family for different a_0 and obtain the bounds and snugness, which are shown in Table 1. From the comparison of the GMW family (with

coefficients determined by the following filtering scheme are corresponding to the effective signal. Another important consideration for using frame is the redundancy, which is particularly useful in noise suppression (Zhang and Ulrych, 2003).

Table 1. Frame bounds and snugness of the wavelet family.

a_0	Morlet Wavelet Family			GMW Family		
	A	B	δ	A	B	δ
2	0.019386	0.564259	0.933569	6.389432	6.903057	0.038640
$2^{1/2}$	0.382460	0.592806	0.215680	13.291070	13.301088	0.000377
$2^{1/3}$	0.717034	0.746598	0.020199	19.944049	19.944188	0.000004
$2^{1/4}$	0.974665	0.976844	0.001117	26.592157	26.592159	0.000000
$2^{1/5}$	1.219642	1.219744	0.000042	33.240198	33.240198	0.000000
$2^{1/6}$	1.463630	1.463634	0.000001	39.888237	39.888237	0.000000
$2^{1/7}$	1.707570	1.707570	0.000000	46.536277	46.536277	0.000000
$2^{1/8}$	1.951509	1.951509	0.000000	53.184316	53.184316	0.000000

The distribution of effective signal

When a noisy signal is projected to the time-scale domain spanned by a proper wavelet frame atom $\psi_{m,n}$, the energy distribution of the effective signal will be confined in a small close subspace V of the time-scale domain, while the energy distribution of the noise will disperse in a larger close subspace V′, even in the whole time-scale space. In other words, the effective signal maps to a relatively small number of significant coefficients, while the energy of the noise spreads more or less evenly among all coefficients. If the subspace V is determined, i.e., the coefficients corresponding to the effective signal are obtained, and the rest of coefficients corresponding to the noise are set to be zero, the noise will be suppressed in the time-scale domain and the signal-to-noise ratio (SNR) will be improved (Wang and Gao, 2013).

To determine the distribution of the effective signal, we introduce a filtering scheme as follows:

1. Project the data contaminated with noise onto the wavelet frame. We

determine the scope of m and n in eq. (18). The range of n corresponding to the translation factor t is determined according to the time coverage of data. Following the method of Meyers et al. (1993), we map the wavelet scale a to the equivalent frequency (see Appendix). According to the frequency coverage of the data, we get the range of m corresponding to the scale factor a.

2. Manipulate a percentage thresholding strategy to the coefficients in time-scale domain. The soft and hard thresholding operators are defined as

$$S_\lambda(u) = \begin{cases} u - \lambda(u/|u|) & \text{if } |u| \geq \lambda \\ 0 & \text{if } |u| < \lambda \end{cases}, \tag{20}$$

and

$$H_\lambda(u) = \begin{cases} u & \text{if } |u| \geq \lambda \\ 0 & \text{if } |u| < \lambda \end{cases}, \tag{21}$$

where λ is a positive threshold parameter, given by

$$\lambda = p \cdot \max_{m,n}\{|C_{m,n}|\} . \tag{22}$$

In eq. (22), the parameter p is a user defined percentage.

Through the filtering scheme, the coefficients corresponding to the "cleaned" scalogram is obtained, which leads to a scalogram with reduced noise. Fig. 3 (top) shows the wavelet scalogram of the noise-free signal, a 50-Hz Ricker wavelet. The scalogram of the noisy signal with an SNR of 5 dB is given in Fig. 3 (middle). Notice the effective signal is obscured by the noise. Fig. 3 (bottom) shows the cleaned scalogram calculated after the filtering process, which reveals the signal clearly.

With the coefficients corresponding to the "cleaned" scalogram, we can calculate the analytic counterpart of the "cleaned" signal using eq. (7) and the instantaneous frequency can be calculated from eqs. (8) and (9).

EXAMPLES AND DISCUSSIONS

To illustrate the different methods, we take a piece of a synthetic seismic trace obtained by convolving a 50-Hz Ricker wavelet with synthetic reflectivity. The noisy-free signal, signal plus Gaussian noise with the SNR of 5 dB are shown in Figs. 4a and 4b. Figs. 4c and 4e give the IF of the noise-free signal calculated by conventional HT method and the proposed approach, respectively.
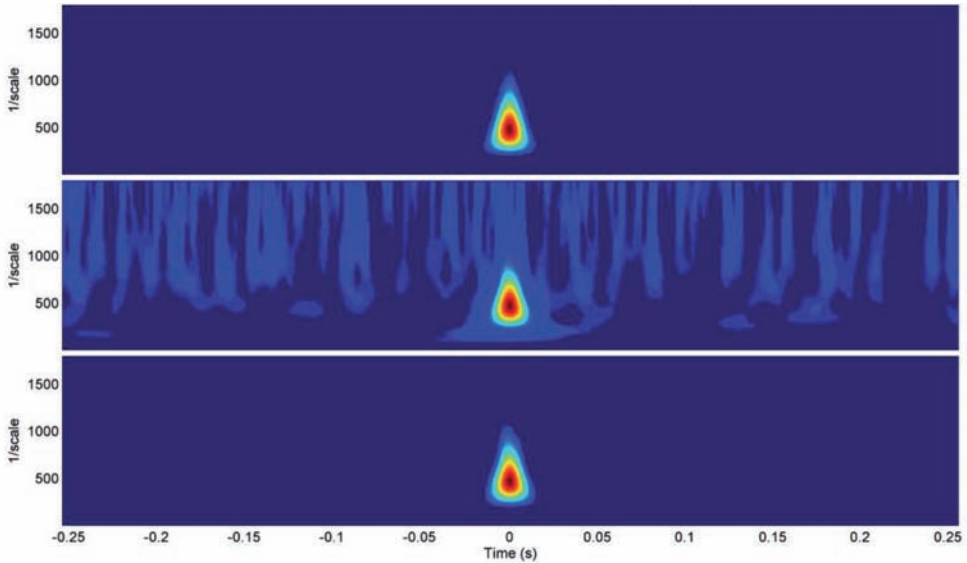
Fig. 3. (a) The noise-free wavelet scalogram (top) and the noisy wavelet scalogram (middle). Through the filtering scheme, the corresponding cleaned scalogram is obtained (bottom).

In the proposed approach, we use the GMW with $\beta = 1$, and $\gamma = 3$. For noise-free signals, the IF is calculated direct using eqs. (6)-(9). The resulting IFs are identical. Both the two methods can give high precision of the IF estimate when it is noise free.

However, when the observed signal is noisy, the IF obtained using the conventional method is inaccurate. Figs. 4d and 4f shows the IFs calculated by conventional HT method and the proposed approach, respectively. In the proposed approach, we project the test signal onto the wavelet frame by eq.(18), using the GMW with $\beta = 1$, and $\gamma = 3$. The range of n is determined according to the time coverage of the record. The range of m is determined by the frequency coverage 1-150 Hz. The user defined percentage p is chosen to be 10%. Through the filtering scheme, we determine the distribution of the effective signal and calculate the analytic counterpart corresponding to the "cleaned" signal using eq. (7). Finally, we get the IF using eq. (9). As can be seen in Fig. 4d, using the conventional HT method, the IF of the effective signal is completely hidden visually due to the noise. However, the result obtained by the proposed approach shown in Fig. 4f reveals the IF of effective signal very well.

To evaluate the robustness against noise of the IFs obtained by different approaches, the signal-to-noise ratio of IF (Wang and Gao, 2013) is defined by
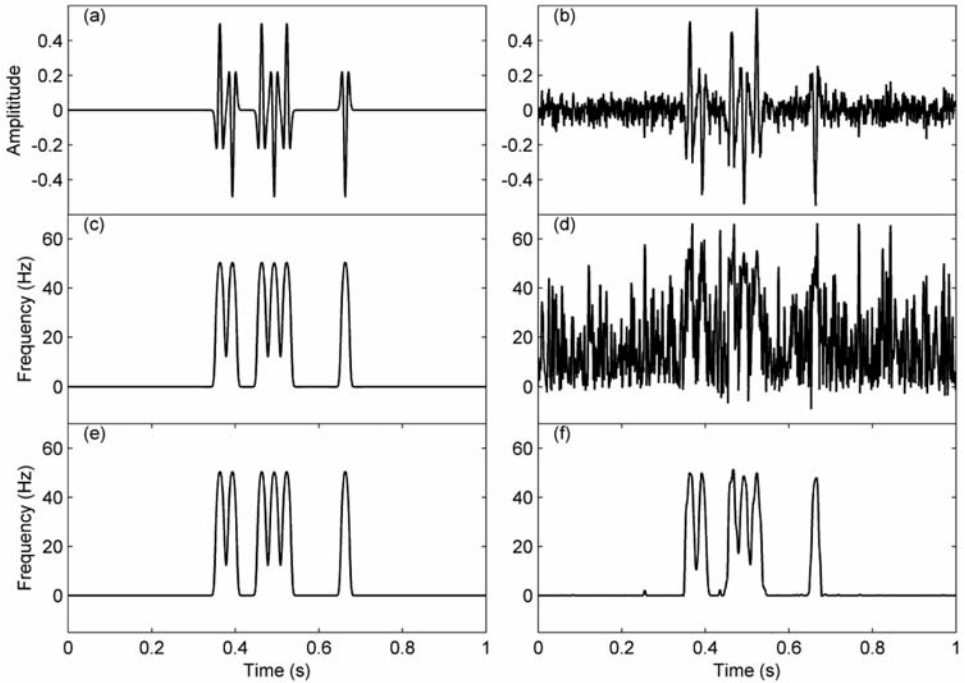
Fig. 4. Test signals and the IFs obtained by different methods. (a) The noise-free synthetic seismic trace. (b) The synthetic seismic trace with noise (SNR = 5 dB). The IFs of the test signal shown in (a) and (b), calculated by conventional HT method, are depicted in (c) and (d). Finally, (e) and (f) show the IFs of test signals calculated by the proposed approach.

$$\text{FSNR} = 10\log_{10}(\|f_0\|^2 / \|f_n - f_0\|^2)(\text{dB}) \quad , \tag{23}$$

where f_0 is the IF of noisy-free signal and f_n is the IF of the noisy signal.

Next, we add Gaussian noise to the noisy-free signal in Fig. 4a with SNRs of 10 dB, 5 dB, and 1 dB. Three noisy synthetic data is presented in Fig. 5. We calculate the IFs of the noisy signal by the proposed approach with hard and soft thresholding in our filtering scheme, respectively. The parameters of the GMW, the range of m and n, and the user defined percentage are the same as in Fig. 4. The resulting IFs are illustrated in Fig. 6, together with the IFs extracted by the conventional HT method. Besides, the FSNRs are listed in Table 2. Comparing with the conventional HT method, the proposed approach significantly improves the FSNRs, even for data contaminated by strong noise. Furthermore, better estimates are obtained using the soft-thresholding than that using the hard-thresholding.
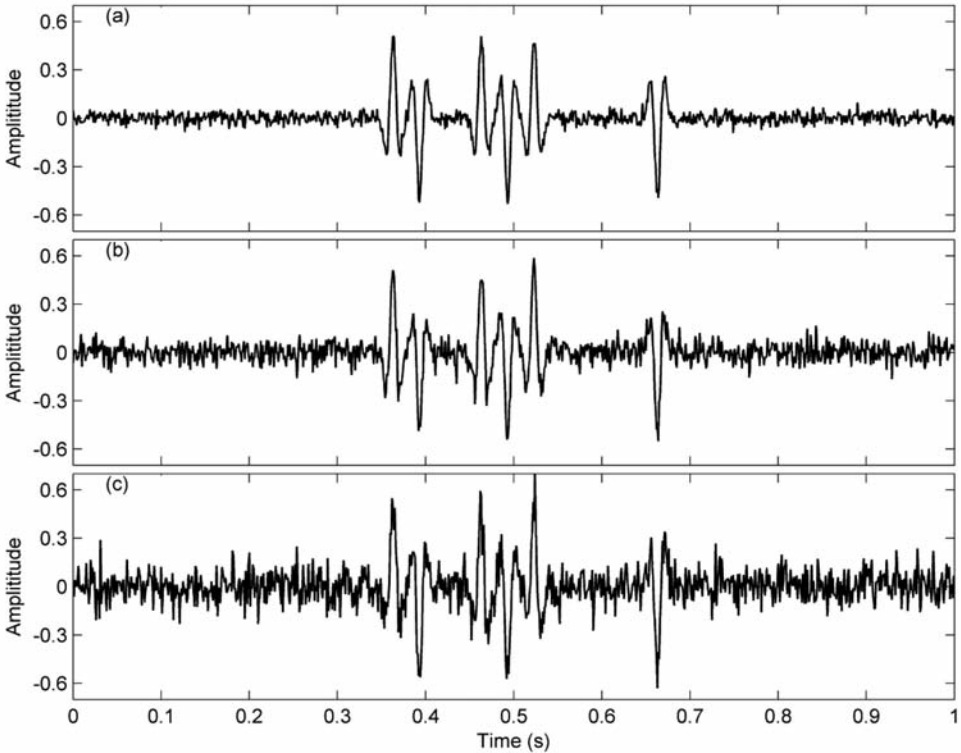
Fig. 5. The noisy test signals at SNRs of (a) 10 dB, (b) 5 dB and (c) 1 dB.

Table 2. The FSNRs of different methods (dB).

SNR(dB)	HT method	Proposed approach using hard-thresholding	Proposed approach using soft-thresholding
10	5.4000	18.9076	23.4937
5	−1.8547	15.6165	18.2455
1	−4.4549	9.4562	15.5099

Subsequently, Figs. 7a and 7b present the IFs of noisy signal at 10 dB SNR obtained by the proposed approach with GMW and Morlet wavelet, respectively. To ensure its analyticity, the carrier wave frequency of Morlet wavelet is set to be 6. The other parameters are the same as in Fig. 4. In the filtering process, the soft-thresholding is employed. The FSNRs are 23.4937 and 13.8837, which shows the better performance of the GMW.

   To further demonstrate the effectiveness of the proposed approach, we apply it to a stacked real 3D seismic data. Fig. 8a shows a profile of the 3D data, Fig. 8b illustrates the IF obtained by conventional HT method, and Fig. 8c presents the IF obtained using the proposed approach. Parameters of the GMW are the same as mentioned above. In the filtering scheme, the range of are determined according to the frequency coverage of the data, which is 1-60 Hz. The percentage of the soft-thresholding strategy is 5%. We can observe high frequencies caused by thin bed reflectivity interferences at 1.75 s, 2 s and 2.25 s. The low-frequency anomaly is shown at 1.90-1.95 s (indicated by arrows). Such anomalous low-frequency shadows are caused by abnormally high attenuation of high-frequency energy in the gas reservoir and can be used as indicators of hydrocarbon (Chopra and Marfurt, 2005). The presence of such a gas reservoir is confirmed by well A - a prolific gas well drilled through the anomaly. It can be noted clearly that the abnormal region is more distinct in Fig. 8c due to the better anti-noise performance of the proposed approach.
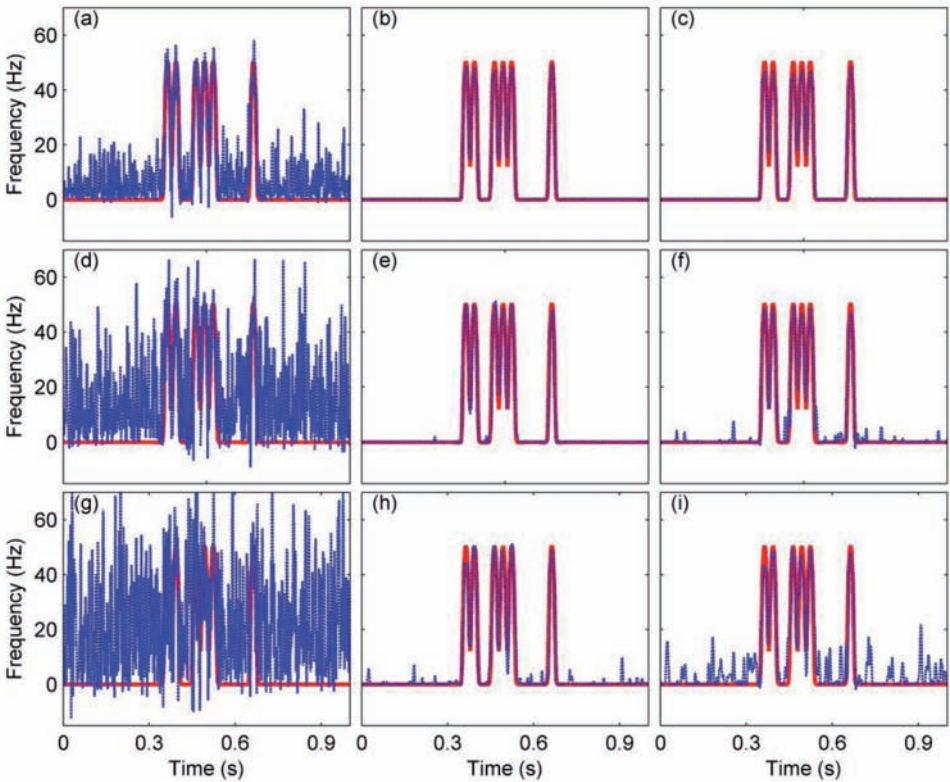

Fig. 6. The IFs of test signals obtained by different methods. The SNRs of the test signal decrease from top to bottom, which take on the values 10 dB, 5 dB and 1 dB. The red line corresponds to the IFs of noisy-free signals from Fig. 4. From left to right, the blue line corresponds to the IFs of noisy signals obtained by conventional HT method, the proposed approach with soft-thresholding and the proposed approach with hard-thresholding.

The filtering scheme in this paper is based on the Gaussian distribution hypothesis of the noise. According to the central limit theorem, the sum of a sufficient number of independent random variables tends to the Gaussian distribution. Therefore, the signal and noise are assumed to satisfy the central limit theorem in most cases in the practical application, especially for the stacked seismic data.

Clearly, this is work in progress. Although the Gaussian noise model can be a good description of most of the system models, there are often non-Gaussian noises in practice. For example, pre-stack seismic data may contain a variety of non-Gaussian noise due to various clutters and man-made noise in seismic data acquisition, and the limited seismic data acquisition is difficult to satisfy the central limit theorem. So the scheme based on Gaussian assumption is difficult to reflect the stratigraphic anomalies accurately. Therefore, directions for future work include exploring the actual noise to design an efficient algorithm for non-Gaussian noise.
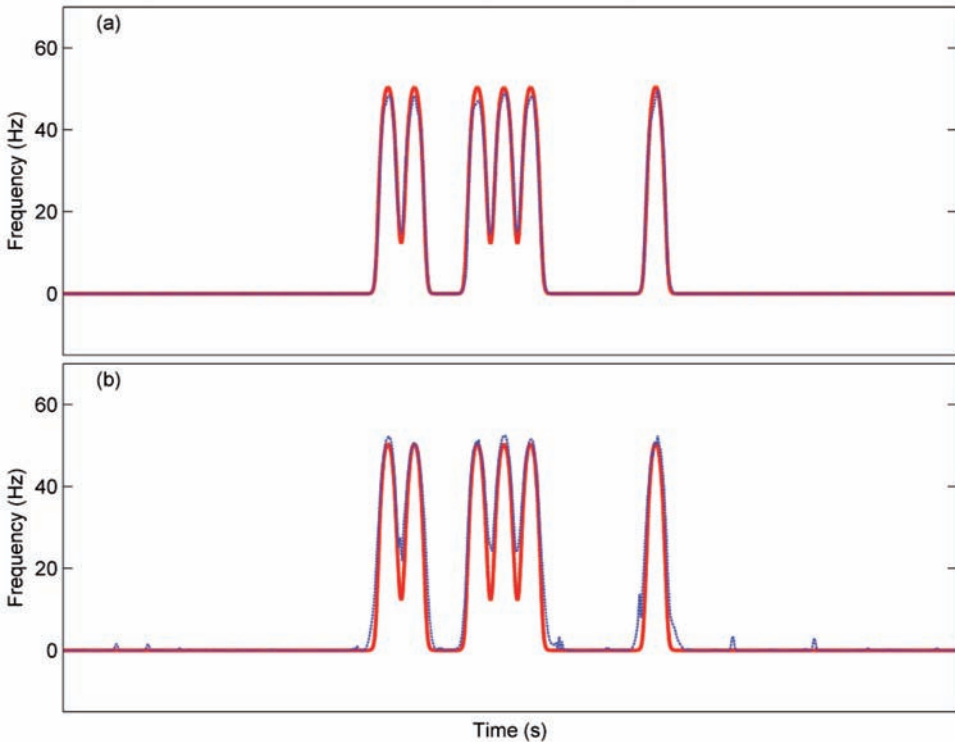

Fig. 7. The IFs of test signals at an SNR of 10 dB. The red line corresponds to the IFs of noisy-free signals from Fig. 4. The blue line corresponds to the IFs of the noisy signals obtained by the proposed approach using (a) GMW and (b) Morlet wavelet.
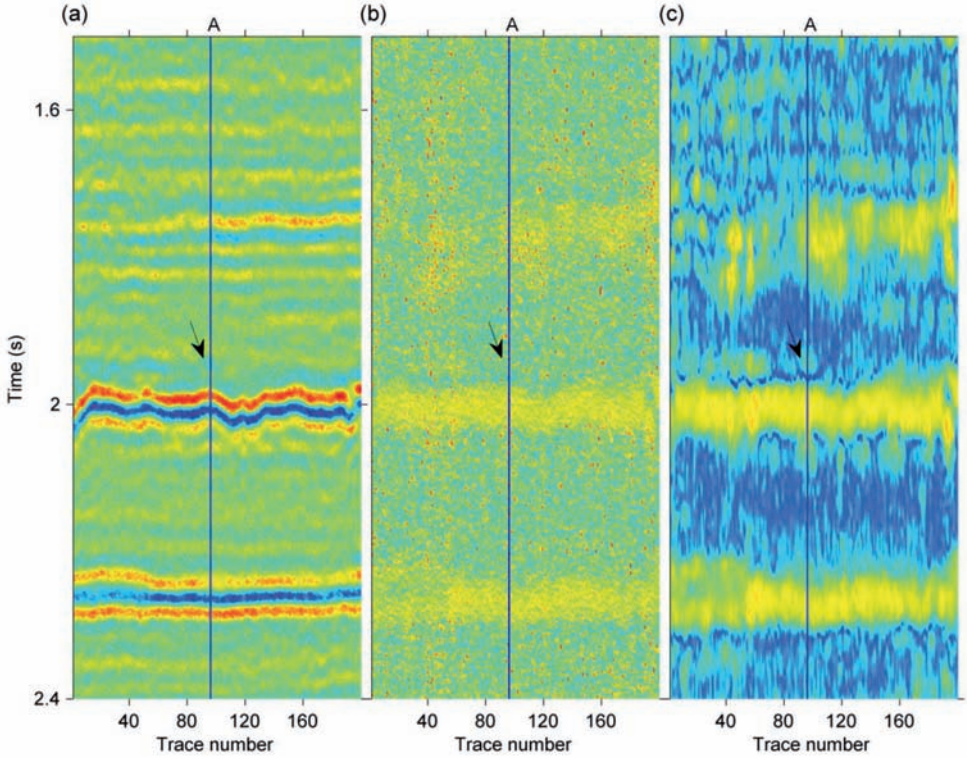
Fig. 8. Example on real data. (a) A profile of the data set which through a prolific gas well A. IF calculated by (b) conventional HT method, and (c) the proposed approach. The arrows indicate the location of the low-frequency anomaly due to the gas reservoirs.

CONCLUSIONS

We have proposed a wavelet frame based approach for the instantaneous attributes estimation. The GMWs have been used as the atom of wavelet frame in the procedure. Owing to the desirable properties, the GMWs exhibit better behaviors than the popular Morlet wavelet. To determine the distribution of the effective signal, we have introduced a filtering scheme. In the filtering process, we have employed a percentage thresholding strategy. The soft-thresholding provides better performance than hard-thresholding. The IFs estimated by the proposed approach are robust for noisy data, even for data at low SNR. The results from both synthetic record and filed data show that the proposed approach outperforms the conventional HT method.

ACKNOWLEDGEMENTS

REFERENCES

Antoine, J.P., Murenzi, R., Vandergheynst, P. and Ali, S.T., 2004. Two-dimensional Wavelets and Their Relatives. Cambridge University Press, Cambridge.
Barnes, A.E., 1992. Short Note The calculation of instantaneous frequency and instantaneous bandwidth. Geophysics, 57: 1520-1524.
Barnes, A.E., 1996, Theory of 2-D complex seismic trace analysis. Geophysics, 61: 264-272.
Boashash, B., 1992. Estimating and interpreting the instantaneous frequency of a signal. I. Fundamentals. Proc. IEEE, 80: 520-538.
Chopra, S. and Marfurt, K.J., 2005. Seismic attributes - A historical perspective. Geophysics, 70 (5): 3SO-28SO.
Duffin, R.J. and Schaeffer, A.C., 1952. A class of nonharmonic Fourier series. Transact. Am. Mathemat. Soc., 72: 341-366.
Fomel, S., 2007. Local seismic attributes. Geophysics, 72 (3): A29.
Fomel, S., 2012. Seismic data decomposition into spectral components using regularized nonstationary autoregression. Expanded Abstr., 82nd Ann. Internat. SEG Mtg., La Vegas.
Gabor, D., 1946. Theory of communication. Part 1: The analysis of information. J. Instit. Electr. Engin., 93 (26): 429-441.
Gao, J., Dong, X., Wang, W.B., Li, Y. and Pan, C., 1999. Instantaneous parameters extraction via wavelet transform. IEEE Transact. Geosci. Remote Sens., 37: 867-870.
Gao, J., Yang, S., Wang, D. and Wu, R., 2011. Estimation of quality factor Q from the instantaneous frequency at the envelope peak of a seismic signal. J. Computat. Acoust., 19: 155-179.
Han, J. and van der Baan, M., 2011. Empirical mode decomposition and robust seismic attribute analysis. Recovery-2011 CSPG CSEG CWLS Convention, Calgary.
Hardage, B.A., 2010. Hilbert transform remains a valuable tool.
    http://www.aapg.org/explorer/2010/06jun/geocorner0610.cfm.
Hardy, H., Beier, R.A. and Gaston, J.D., 2003. Frequency estimates of seismic traces. Geophysics, 68: 370-380.
Holschneider, M. and Kon, M.A., 1996. Wavelets: An Analysis Tool. Oxford University Press, Oxford.
Huang, J.W. and Milkereit, B., 2009. Empirical mode decomposition based instantaneous spectral analysis and its applications to heterogeneous petrophysical model construction. Proc. 2009 CSPG CSEG CWLS Conv., Calgary: 205-210.
Lilly, J.M. and Olhede, S.C., 2009. Higher-order properties of analytic wavelets. IEEE Transact. Sign. Process., 57: 146-160.
Lilly, J.M. and Olhede, S.C., 2010. On the analytic wavelet transform. IEEE Transact. Informat. Theory, 56: 4135-4156.
Lilly, J.M. and Olhede, S.C., 2012. Generalized Morse wavelets as a superfamily of analytic wavelets. IEEE Transact. Sign. Process., 60: 6036-6041.
Mallat, S.G., 2009. A wavelet tour of signal processing: the sparse way. Academic Press Inc., New York.
Matheney, M.P. and Nowack, R.L., 1995. Seismic attenuation values obtained from instantaneous-frequency matching and spectral ratios. Geophys. J. Internat., 123: 1-15.

Meyers, S.D., Kelly, B.G. and O'Brien, J.J., 1993. An introduction to wavelet analysis in oceanography and meteorology: With application to the dispersion of Yanai waves. Monthly Weather Rev., 121: 2858-2866.

Olhede, S.C. and Walden, A.T., 2002. Generalized morse wavelets. IEEE Transact. Sign. Process., 50: 2661-2670.

Olhede, S.C. and Walden, A.T., 2003. Polarization phase relationships via multiple Morse wavelets. I. Fundamentals. Proc. Roy. Soc. London, Series A: Mathemat., Phys. Engin. Sci., 459 (A): 413-444.

Picinbono, B., 1997. On instantaneous amplitude and phase of signals. IEEE Transact. Sign. Process., 45: 552-560.

Steeghs, P. and Guy, D., 2001. Seismic sequence analysis and attribute extraction using quadratic time-frequency representations. Geophysics, 66: 1947-1959.

Taner, M.T., 2001. Seismic Attributes. CSEG Recorder, 26 (7): 48-56.

Taner, M.T., Koehler, F. and Sheriff, R., 1979. Complex seismic trace analysis. Geophysics, 44: 1041-1063.

Vakman, D., 1996. On the analytic signal, the Teager-Kaiser energy algorithm, and other methods for defining amplitude and frequency. IEEE Transact. Sign. Process., 44: 791-797.

Ville, J., 1948. Theorie et applications de la notion de signal analytique. Cables Transmiss., 2: 61-74.

Wang, P. and Gao, J., 2013. Extraction of instantaneous frequency from seismic data via the generalized Morse wavelets. J. Appl. Geophys., 93: 83-92.

Wang, X., Gao, J. and Chen, W., 2012. A new tiling scheme for 2-D continuous wavelet transform with different rotation parameters at different scales resulting in a tighter frame. IEEE Sign. Process. Lett., 19: 407-410.

Yang, S. and Gao, J., 2010. Seismic attenuation estimation from instantaneous frequency. IEEE Geosc. Remote Sens. Lett., 7: 113-117.

Zhang, R. and Ulrych, T.J., 2003. Physical wavelet frame denoising. Geophysics, 68: 225-231.

Zhou, Y., Chen, W., Gao, J. and He, Y., 2012. Application of Hilbert-Huang transform based instantaneous frequency to seismic reflection data. J. Appl. Geophys., 82: 68-74.

APPENDIX

WAVELET SCALES AND FREQUENCY OF THE GMW

The relationship between the equivalent frequency and the wavelet scale is derived as follows. We choose a signal $s(t) = e^{i\omega_0 t}$ of a known frequency ω_0 and compute the scale a at which the wavelet power spectrum reaches its maximum.

We take the CWT using eq. (6)

$$W_\psi(t,a) \equiv (1/a) \int_{-\infty}^{+\infty} s(\tau)\psi^*[(\tau - t)/a]d\tau$$

$$= (1/2\pi) \int_{-\infty}^{+\infty} S(\omega)\Psi^*(a\omega)e^{i\omega t}d\omega$$

$$= \Psi^*(a\omega_0)e^{i\omega_0 t} \quad . \tag{A-1}$$

The wavelet power spectrum is

$$|W_\psi(t,a)|^2 = |\Psi(a\omega_0)|^2 .$$ (A-2)

For the GMW,

$$\Psi_{\beta,\gamma}(\omega) = U(\omega)\alpha_{\beta,\gamma}\omega^\beta e^{-\omega^\gamma} .$$ (A-3)

Substituting into eq. (A-2), we obtain

$$|W_\psi(t,a)|^2 = \alpha_{\beta,\gamma}^2(a\omega_0)^{2\beta}e^{-2(a\omega_0)^\gamma}$$

$$= \alpha_{\beta,\gamma}^2 x^{2\beta}e^{-2x^\gamma} ,$$ (A-4)

where $x = a\omega_0$. Let

$$F_{\beta,\gamma}(x) \equiv x^{2\beta}e^{-2x^\gamma} .$$ (A-5)

To find the scale a of maximum correlation, we set the derivative of $\ln F_{\beta,\gamma}(x)$ equal to zero and obtain

$$\partial \ln F_{\beta,\gamma}(x)/\partial x = (2\beta/x) - 2\gamma x^{\gamma-1} = 0 .$$ (A-6)

The solution is

$$x_0 = (\beta/\gamma)^{1/\gamma} .$$ (A-7)

Using $x_0 = a_0\omega_0$ and $\omega_0 = 2\pi f_0$, the relation between wavelet scale and frequency is obtained:

$$a_0 = (\beta/\gamma)^{1/\gamma}/2\pi f_0 .$$ (A-8)